HHS Public Access

Author manuscript

Invest Radiol. Author manuscript; available in PMC 2021 November 01.

Published in final edited form as:

Invest Radiol. 2020 November ; 55(11): 727–735. doi:10.1097/RLI.0000000000000698.

Inversion recovery susceptibility weighted imaging with enhanced T_2-weighting (IR-SWIET) at 3 tesla improves visualization of subpial cortical multiple sclerosis lesions

Erin S Beck, MD, PhD[1], **Neville Gai, PhD**[2], **Stefano Filippini, MD**[3,4], **Josefina Maranzano, MD, PhD**[5], **Govind Nair, PhD**[6], **Daniel S Reich, MD, PhD**[7]

[1]Clinical Neuroimmunology Fellow, Translational Neuroradiology Section (TNS), National Institute of Neurological Disorders and Stroke (NINDS), National Institutes of Health (NIH), Bethesda, MD, USA

[2]Staff Scientist, Radiology and Imaging Sciences, Clinical Center, NIH, Bethesda, MD, NIH

[3]Visiting Fellow, Translational Neuroradiology Section (TNS), National Institute of Neurological Disorders and Stroke (NINDS), National Institutes of Health (NIH), Bethesda, MD, USA

[4]Neurology Resident, Department of Neurosciences, Drug, and Child Health, University of Florence, Florence, Italy

[5]Assistant Professor, University of Quebec in Trois-Rivieres, Trois-Rivieres, Quebec, Canada

[6]Staff Scientist, Translational Neuroradiology Section (TNS), National Institute of Neurological Disorders and Stroke (NINDS), National Institutes of Health (NIH), Bethesda, MD, USA

[7]Senior Investigator, Translational Neuroradiology Section (TNS), National Institute of Neurological Disorders and Stroke (NINDS), National Institutes of Health (NIH), Bethesda, MD, USA

Abstract

Objectives: Cortical demyelination is common in multiple sclerosis (MS) and can be extensive. Cortical lesions contribute to disability independently from white matter lesions and may form via a distinct mechanism. However, current magnetic resonance imaging (MRI) methods at 3 tesla (3T) are insensitive to cortical, and especially subpial cortical, lesions. Subpial lesions are well-seen on T_2* weighted imaging at 7 tesla (7T), but T_2* weighted methods on 3T scanners are limited by poor lesion-to-cortex and cerebrospinal fluid (CSF)-to-lesion contrast. We aimed to develop and evaluate a CSF-suppressed, T_2*-weighted sequence optimized for subpial cortical lesion visualization.

Materials and methods: We developed a new MRI sequence, Inversion Recovery Susceptibility Weighted Imaging with Enhanced T_2-Weighting (IR-SWIET, 0.8mm x 0.8mm in plane, 0.64mm slice thickness with whole brain coverage, acquisition time ~5 min). We compared cortical lesion visualization independently on IR-SWIET (median signal from four acquisitions),

Corresponding author: Daniel S Reich, Building 10, Rm 5c103, 10 Center Dr, Bethesda, MD 20892, Phone: 301-496-1801, Fax: 301-402-0373, daniel.reich@nih.gov.

magnetization-prepared 2 rapid acquisition gradient echoes (MP2RAGE), double inversion recovery (DIR), T_2* weighted segmented echo-planar imaging (T_2*wEPI), and phase sensitive inversion recovery (PSIR) images for ten adults with MS. We also identified cortical lesions with a multicontrast reading of IR-SWIET (median of two acquisitions), MP2RAGE, and fluid attenuated inversion recovery (FLAIR) images for each case. Lesions identified on 3T images were verified on "gold standard" 7T T_2* and MP2RAGE images.

Results: Cortical, and particularly subpial, lesions appeared much more conspicuous on IR-SWIET compared to other 3T methods. A total of 101 true positive subpial lesions were identified on IR-SWIET (average per-participant sensitivity vs 7T, 29 ± 8%) vs 36 on MP2RAGE (5 ± 2%, comparison to IR-SWIET sensitivity p=0.07), 17 on FLAIR (2 ± 1%, p<0.05), 28 on DIR (6 ± 2%, p<0.05), 42 on T_2*wEPI (11 ± 5%, p<0.05), and 13 on PSIR (4 ± 2%, p<0.05). When a combination of IR-SWIET, MP2RAGE, and FLAIR images was used, a total of 147 subpial lesions (30 ± 5%) were identified, versus 83 (16 ± 3%, p<0.01) on a combination of DIR, MP2RAGE, and FLAIR. More cases had at least one subpial lesion on IR-SWIET, and IR-SWIET improved cortical lesion subtyping accuracy and correlation with 7T subpial lesion number.

Conclusions: Subpial lesions are better visualized on IR-SWIET compared to other 3T methods. A 3T protocol combining IR-SWIET with MP2RAGE, in which leukocortical lesions are well seen, improves cortical lesion visualization over existing approaches. IR-SWIET may therefore enable improved MS diagnostic specificity and a better understanding of the clinical implications of cortical demyelination.

Keywords

Neuroimaging; multiple sclerosis; cortical lesions; T_2* weighted magnetic resonance imaging; magnetic susceptibility

Introduction:

While multiple sclerosis (MS) is traditionally thought of as a disease of white matter, cortical lesions are common and often extensive (1–3). Cortical lesions are associated with disability and with progressive forms of MS (4–8). In addition, there is evidence that cortical lesions, and especially subpial cortical lesions that touch the pial surface of the brain, may form independently from white matter lesions, perhaps due to leptomeningeal inflammation (9–12).

Further insight into cortical lesion clinical significance, natural history, and response to treatment has been limited by the insensitivity of current 3 tesla (3T) MRI methods to cortical, and especially subpial, lesions. Double inversion recovery (DIR), a sequence with suppressed cerebrospinal fluid (CSF) and white matter signal, has been used most extensively to study cortical lesions in vivo (13–15). However, this method is limited by low signal and artifacts, yielding false positives. When compared to postmortem pathology, 3T DIR was 83% sensitive for leukocortical lesions, but only 7% sensitive for subpial lesions (16, 17). Phase-sensitive inversion recovery (PSIR) has also been used for cortical lesion visualization at 3T (18–21). While PSIR appears to improve sensitivity to leukocortical lesions, data on improvement in subpial lesion detection has been inconsistent (19, 21).

More recently, T_1 weighted magnetization-prepared 2 rapid acquisition gradient echoes (MP2RAGE, (22)) and its derived images such as bias-free T_1-weighted images and T1-maps (23), have been used for cortical lesion detection at 3T, with a similar cortical lesion detection rate as DIR (23), and at 7T (24).

T_2* weighted methods at 7 tesla (7T) have also been used to image cortical lesions (8, 24–28), with substantial improvement in subpial lesion detection rate in MS compared to 3T (17, 29). The increased sensitivity of T_2* weighting for cortical demyelination at ultra-high field is likely due to a combination of increased sensitivity to loss of myelin as well as to loss of iron (26, 30–33). In addition, ultra-high field strength makes it easier to obtain higher resolution scans due to the increased signal-to-noise ratio (2-fold increase in signal-to-noise ratio at 7T compared to 3T, (34)), enabling detection of smaller lesions. Nevertheless, 3T clinical scanners could potentially be made more sensitive to subpial lesions by increasing the lesion contrast relative to surrounding tissue such as CSF and cortical gray matter through CSF-nulling and optimal parameter selection. Here, we describe the construction and evaluation of a new 3T sequence with enhanced T_2* weighting and suppressed CSF signal (inversion recovery susceptibility weighted imaging with enhanced T_2 weighting, IR-SWIET), which improves subpial cortical lesion detection in MS.

Materials and methods:

Development of a T_2* weighted sequence with suppressed CSF signal:

A pulse sequence was designed to maintain T_2 and T_2* contrast similar to a 3D T_2* weighted sequence. Bloch simulation for IR-SWIET (Figure 1A) shows the signal evolution for gray matter, white matter, and CSF. T_1 and T_2 relaxation times and proton density values from the literature were used (35–38). Acquisition was performed at steady-state.

The T_2* weighted segmented echo-planar imaging (T_2*wEPI) sequence was modified to suppress CSF using 90_x–$180_y(4)$ -90_{-x} T_2-Preparation (T_2-prep) module followed by inversion similar to 3D fluid attenuated inversion recovery (FLAIR) (39). Since magnetization for gray matter recovers at a slower rate than for white matter, gray matter-lesion-white matter T_2 contrast is compromised at CSF null. To compensate for the lower gray matter longitudinal magnetization, additional T_2 weighting with a shorter duration T_2-Prep pulse was introduced prior to echo-planar imaging (EPI) acquisition. This T_2-Prep duration was based on the calculated time at which gray matter and white matter signal are equal based on their initial magnetization values. Vascular signal can show up as hyperintensity and confound lesion detection, so vascular crushing was introduced prior to acquisition to suppress this signal. The final sequence is shown schematically in Figure 1B (40). Improved T_2 weighting was obtained by acquiring the echo train in a centric fashion. An EPI factor of 23 was used, with 22 excitations per inversion and SENSE parallel imaging (2.5x2). The remainder of the optimized IR-SWIET sequence parameters are listed in Table 1.

Data acquisition:

This study was approved by the local institutional review board, and informed consent was obtained from all participants. 10 adults with MS and 2 healthy adults (see Table S1 for cohort details) underwent scans on a 3T scanner (Philips Achieva 3.0 T; Philips Healthcare, Eindhoven, the Netherlands) equipped with a 32-channel head coil. This scan included optimized IR-SWIET, acquired four times in each scanning session, FLAIR, DIR, PSIR, and T_2*wEPI (see Table 1 for sequence parameters). For the MS cases, previously acquired 3T MP2RAGE images (3T Magnetom Skyra, Siemens, Erlangen, Germany, equipped with a 32-channel head coil) and 7T MP2RAGE (acquired four times) and T_2* weighted gradient recalled echo (GRE) images (7T whole-body research system, Siemens, equipped with a single-channel transmit, 32-channel phased array receive head coil) were also used for comparison. 3T MP2RAGE images were acquired 1–7 months (median 3 months) before the 3T Philips scans. 7T scans were acquired 1–7 months (median 4 months) before the 3T Philips scans.

Image processing:

MP2RAGE 3T and 7T processing to generate uniform images was performed on the respective scanners as a part of the Siemens research sequence package (Work-in-Progress Package #900D). IR-SWIET repetitions were coregistered (ANTS (41)), and the voxel-wise median of the first two or all four acquisitions was generated. The 7T MP2RAGE repetitions were similarly coregistered, and the median of all four acquisitions was generated. The median was used, rather than the mean, to decrease the contribution of outlier values that may arise due to noise or motion. All images were aligned to the 7T MP2RAGE uniform denoised images using linear coregistration (AFNI (42)).

Lesion identification and comparison:

Cortical lesions were manually segmented using the software package Display (https://github.com/BIC-MNI/Display) developed at the McConnell Brain Imaging Center of the Montreal Neurological Institute.

Cortical lesions were identified and marked on all 3T images by an experienced neurologist (ESB, with more than 3 years' experience in cortical lesion segmentation). Cortical lesions were identified on 3T IR-SWIET single acquisition (IR-SWIETx1), IR-SWIET median of 2 acquisitions (IR-SWIETx2), IR-SWIET median of 4 acquisitions (IR-SWIETx4, see Figure S1 and Table 2 for comparison of IR-SWIET medians), DIR, PSIR, FLAIR, T2*wEPI, and MP2RAGE images independently in random order, with at least one week in between analysis of each sequence from the same subject. In addition, two 3T multicontrast reads were performed for each subject: (1) IR-SWIETx2, MP2RAGE, FLAIR; (2) DIR, MP2RAGE, FLAIR.

Cortical lesions were segmented on 7T images using both MP2RAGE and T_2*w GRE images. This segmentation was done by two raters independently (ESB and JM, a neuroradiologist with over 15 years' experience (43)), followed by a consensus read by both raters. On 3T and 7T images, cortical lesions were classified as leukocortical, intracortical,

or subpial (2). Lesion volume was calculated for each cortical lesion identified on 7T images using the MP2RAGE images.

Following identification of cortical lesions on all 3T images, each marked lesion was compared to the 7T images used as a “gold standard” for cortical lesion segmentation. Each lesion was classified as a true cortical lesion, a juxtacortical lesion, a false positive if no correlate was seen on 7T images, or a false negative cortical lesion if a lesion was seen on 7T images only in retrospect. Lesions identified on 3T images that were out of the field of view (FOV) on the 7T images (which do not cover the inferior regions of the temporal and occipital lobes) were classified as out-of-FOV and were not included in the quantitative analyses of lesion detection. For lesion detection analyses, cortical lesion subtype was determined based on the appearance of each lesion at 7T, as subtyping was difficult at 3T.

Purely intracortical (i.e., non-subpial) lesions seen on 7T images were virtually undetected on all of the 3T images, with only three intracortical lesions identified on 3T images for all ten MS cases. Thus, intracortical lesions are included in the total cortical lesion analysis but were not separately analyzed.

To determine interrater reliability, cortical lesions were identified by a second rater (SF, a neurologist with 2 years’ experience in MS image analysis) on IR-SWIETx2 images as well as on a multicontrast read of IR-SWIETx2, MP2RAGE, and FLAIR.

Statistics

The Friedman test was used to compare detected lesion number, sensitivity, and volume between individual sequences. Spearman correlation coefficients were calculated when comparing number of subpial lesions identified on 3T vs 7T. A linear mixed effects model was used to determine the effect of 3T sequence on subpial classification accuracy, with subject included in the model as a random intercept. Post-hoc pairwise comparisons between individual sequences and IR-SWIETx4 as well as comparisons between the two multicontrast reads were performed. Intraclass correlation coefficients were determined using a two-way model. As this was an exploratory study, p-values, when <0.05, are reported directly without adjustment for multiple comparisons.

Results:

MS lesions are conspicuous on IR-SWIET images

On IR-SWIET images, there is low contrast between gray and white matter, and the CSF signal is effectively suppressed. MS lesions in the white matter, deep gray matter, brainstem, and cortex are clearly visualized (Figure 2). In many cases, central veins, which are a hallmark of MS lesions (44), can be seen within lesions (Figure 2C,E). However, there is very little differentiation between gray and white matter, making distinction between juxta- and leuko-cortical lesions difficult based solely on the IR-SWIET images. In addition, RF inhomogeneity caused mild signal variations in the central region of the brain, potentially obscuring pathology there. There is also signal loss around the sinuses related to B0 inhomogeneity.

More subpial lesions are detected on IR-SWIET

Images from 10 adults with MS were used to identify cortical lesions independently on IR-SWIETx2 and x4, other state-of-the-art sequences used to detect cortical lesions (DIR, PSIR), and standard clinical MRI sequences (MP2RAGE, FLAIR, T_2*wEPI). A similar number of total cortical lesions were identified on each of the individual 3T sequences (Table 2, Figure 3). While IR-SWIET did not improve detection of leukocortical lesions, there was a significant improvement in subpial lesion detection. A total of 101 true positive subpial lesions (median lesions/case, 5; average per-participant sensitivity vs. 7T, 29%) were detected on IR-SWIETx4, compared to 36 (median 1; sensitivity 5%; p-value vs IR-SWIETx4, p=0.07) on MP2RAGE and 28 (median 1; sensitivity 6%; p-value vs IR-SWIETx4, $p<0.05$) on DIR. The percentage of lesions classified as false positive did not differ between sequences. No cortical lesions were detected on any combination of IR-SWIET images in either of the two healthy volunteers who were scanned. In addition, more cases had at least one subpial lesion on IR-SWIETx4 and IR-SWIETx2 (9 of 10 cases with each sequence) than any of the other 3T sequences: MP2RAGE (6/10), FLAIR (4/10), DIR (6/10), T_2*wEPI (7/10), and PSIR (5/10).

Inclusion of IR-SWIET in multicontrast identification of cortical lesions improves subpial lesion detection

To simulate a real-world scenario in which multiple image types are used to identify cortical lesions, we identified cortical lesions on two multicontrast reads: IR-SWIETx2, MP2RAGE, and FLAIR and DIR, MP2RAGE, and FLAIR. IR-SWIETx2 was used instead of IR-SWIETx4 as the improvement in subpial lesion sensitivity between the two was small and the shorter scan time of IR-SWIETx2 (~10 min vs ~20 min) is more clinically feasible. We compared the lesions identified on the two multicontrast reads with lesions identified on 3T MP2RAGE alone to determine if inclusion of IR-SWIET or DIR, neither of which is used routinely on clinical MRI scans, improves subpial sensitivity over the more standard 3T MP2RAGE sequence. The multicontrast read of IR-SWIETx2, MP2RAGE, and FLAIR improved average cortical lesion sensitivity vs MP2RAGE alone (43% vs 25%, $p<0.05$). The IR-SWIETx2/MP2RAGE/FLAIR multicontrast read was also more sensitive for subpial lesions (30%) compared to DIR/MP2RAGE/FLAIR (16%, $p<0.01$) or MP2RAGE alone (5%, $p<0.01$) (Table 2, Figure 3). At least one subpial lesion was detected in more cases on the multicontrast read that included IR-SWIETx2 (9/10) than on the read that included DIR (8/10).

Interrater reliability for cortical lesion identification using IR-SWIET

To determine the interrater reliability of cortical lesion detection for IR-SWIET, a second rater identified cortical lesions on IR-SWIETx2 as well as on a multicontrast read of IR-SWIETx2, MP2RAGE, and FLAIR. 36% of true lesions identified on IR-SWIETx2 were identified by both raters versus 48% on IR-SWIETx2/MP2RAGE/FLAIR. This is similar to what we observed for our 7T rating, in which 45% of lesions confirmed on our consensus read were initially identified by both raters. Despite the missed lesions by each rater, the intraclass correlation coefficient (ICC) for total cortical lesion number was high for both IR-

SWIETx2 (0.83) and IR-SWIETx2/MP2RAGE/FLAIR (0.89), and comparable to the ICC for total cortical lesion counts at 7T (0.91) (Table 3).

Contribution of lesion size to cortical lesion detection

Although IR-SWIET increases the number of detected subpial lesions substantially, the number of subpial lesions identified on 3T remained lower than the number detected on 7T. A maximum of 30% of subpial lesions identified on 7T images were detected on 3T images using a combination of IR-SWIETx2, MP2RAGE, and FLAIR. We investigated the impact of cortical lesion size measured on 7T MP2RAGE on the detectability of lesions at 3T. For each sequence, the average size of detected lesions was greater than the average size of undetected lesions ($p<0.001$ for each sequence, Figure S2). When sensitivity of each of the 3T sequences for subpial lesions was calculated in terms of cortical lesion volume rather than number, we found a similar relationship between the 3T sequences, with generally higher sensitivity when calculated by volume, likely due to higher sensitivity for larger subpial lesions (Figure S2). There was no difference between the average size of detected lesions among individual 3T sequences (Figure S2).

IR-SWIET improves subpial lesion classification

Cortical lesion subtype categorization was done for all of the above analyses based on 7T images. Cortical lesion subtype was also determined on 3T images. We determined the percentage of subpial lesions identified on images from each 3T sequence that were correctly classified as subpial on the 3T read. On IR-SWIETx4, 88 ± 5% of identified subpial lesions were categorized correctly, vs 79 ± 13% on IR-SWIETx2, 52 ± 16% on MP2RAGE ($p<0.01$ vs IR-SWIETx4), 45 ± 20% on FLAIR ($p<0.01$), 53 ± 16% on DIR ($p<0.01$), 98 ± 1% on T_2*wEPI ($p=0.58$), and 77 ± 14% on PSIR ($p=0.50$) (Figure 4A). On the IR-SWIETx2/MP2RAGE/FLAIR multicontrast read, an average of 84 ± 6% of the detected subpial lesions were correctly classified, versus only 40 ± 12% on the DIR/MP2RAGE/FLAIR multicontrast read ($p<0.01$) (Figure 4A). Less than 5% of true cortical lesions were misclassified as subpial on any of the individual sequence or multicontrast reads.

IR-SWIET improves 3T-7T subpial correlation

We next examined the relationship between the number of subpial lesions identified on 7T and the number of lesions identified as subpial on each of the 3T sequences and the two multicontrast reads. False positive and incorrectly classified lesions identified on 3T were included in this analysis. For the single 3T sequences, correlation was highest for IR-SWIETx2 ($r=0.89$, $p<0.01$). Correlations for other sequences were as follows: IR-SWIETx4 ($r=0.85$, $p<0.01$), T_2*wEPI ($r=0.70$, $p<0.05$), FLAIR ($r=0.70$, $p<0.05$), PSIR ($r=0.61$, $p=0.07$), MP2RAGE ($r=0.60$, $p=0.07$), and DIR ($r=0.56$, $p=0.09$) (Figure 4B). The correlation for each of the multicontrast reads were similarly high ($r=0.86$, $p<0.01$ for IR-SWIETx2/MP2RAGE/FLAIR and $r=0.94$, $p<0.001$ for DIR/MP2RAGE/FLAIR) (Figure 4B).

Discussion:

In this study, we report the development and optimization of a new MRI sequence, IR-SWIET, with high-resolution, CSF-suppressed T_2* weighted images for better visualization of MS cortical lesions, especially subpial lesions, at 3T. White matter, deep gray matter, brainstem, and cerebellar lesions are also visible on IR-SWIET images at 3T. In addition, central veins are clearly seen in white matter and infratentorial lesions. While the sequence was developed and tested in MS, we expect that it will have broad applicability for detection and characterization of a wide range of central nervous system disorders in which the cortex may be affected — potentially including infarction, neoplasm, epilepsy, and congenital/developmental anomalies.

In MS, when cortical lesion identification was compared between IR-SWIET and other 3T methods, we found that more leukocortical lesions were identified with MP2RAGE than with IR-SWIET. Most of the leukocortical lesions seen on MP2RAGE were visible in retrospect on IR-SWIET. These lesions were likely missed on the initial IR-SWIET review due to the lack of cortex-white matter contrast on these images, leading to misclassification of leukocortical lesions as juxtacortical or subcortical lesions, which were not counted.

In contrast, subpial lesion sensitivity was higher for IR-SWIET than for FLAIR, DIR, T_2*wEPI, and PSIR. Although there was no statistical difference for the comparison with MP2RAGE, our qualitative impression, which might be borne out quantitatively in a larger study, is that subpial lesions are less conspicuous on MP2RAGE (example in Fig. 3). In addition, more subpial lesions were identified on a multicontrast read that included IR-SWIETx2, MP2RAGE, and FLAIR compared to the multicontrast read that included DIR, MP2RAGE, and FLAIR, and more cases were found to have subpial lesions with IR-SWIET, both on individual sequence and multicontrast reads. Interrater reliability was also better for the multicontrast read of IR-SWIETx2, MP2RAGE, and FLAIR compared to IR-SWIETx2 alone, likely because subtle lesions are more likely to be identified when seen on multiple contrasts. Finally, subpial lesion classification was much more accurate using IR-SWIETx2, MP2RAGE, and FLAIR than with DIR, MP2RAGE, and FLAIR.

Nevertheless, the sensitivity of any combination of the 3T scans for subpial lesions remained low compared to the 7T multicontrast read (at most 30% with the IR-SWIETx2, MP2RAGE, and FLAIR multicontrast read). This is to some extent expected given the improvement in signal-to-noise and contrast-to-noise ratios at ultra-high field, and differences in imaging resolution (0.5mm isotropic sequences at 7T vs 0.8-1mm in plane resolution at 3T). In addition, the total acquisition time was much higher on 7T compared to 3T: a total of 1hr 15 min for 7T vs 25 min for 3T (IR-SWIETx2, MP2RAGE, and FLAIR). While some of the lesions seen on 7T were likely missed on 3T due to their small size, other lesions were likely missed due to low contrast between some cortical lesions and normal appearing gray matter. Finally, the 7T “gold standard” lesions were identified by two raters vs. only one rater for the 3T images. Even at 7T, there is significant interrater variability, usually due to lesions missed by a single rater but confirmed as true lesions on a consensus read (24, 43).

Despite the missed subpial lesions on 3T images, the correlation between the number of subpial lesions identified on IR-SWIET images and the number identified on 7T images was high compared to other 3T sequences. This comparison included false positive 3T lesions and lesions misclassified as subpial on 3T, and thus simulates a scenario in which no 7T gold standard exists for comparison. Given the close correlation between 3T and 7T subpial lesion number using IR-SWIET and the improved accuracy of subpial classification using this method, associations between subpial lesion number measured on 3T IR-SWIET and clinical and MRI metrics are likely to be similar to what would be found if subpial lesions were measured on 7T images, but with the advantages that 3T MRI is much more accessible in a clinical setting, total scan time is much shorter, and whole-brain coverage is more easily attained.

The focus in this study was on cortical lesion visualization, but white matter and brainstem lesions are also very prominent on IR-SWIET images, as are central veins within lesions. Further dedicated analysis into the utility of this sequence more broadly for MS — where it could potentially substitute for FLAIR and/or susceptibility-weighted imaging — as well as for other conditions, is warranted. In addition, phase images, which were not analyzed here, or a combination of phase and magnitude images, may provide additional information on lesion characterization. Finally, since T_1 relaxation plays a role in the IR-SWIET contrast mechanism, the utility of post-gadolinium IR-SWIET acquisition for detection of both parenchymal and leptomeningeal enhancement (45) could also be explored.

In summary, IR-SWIET, when combined with a T_1-weighted sequence such as MP2RAGE, allows effective cortical lesion visualization and is much more feasible than 7T methods. We favor a median of two IR-SWIET acquisitions for the best balance of subpial lesion sensitivity and scan time. Associations between subpial cortical lesions, disability, and progressive forms of MS can now be determined in much larger cohorts of patients than has been possible with 7T and with much higher sensitivity and accuracy than has been possible with current 3T methods. Cortical lesions detected with IR-SWIET could also be incorporated into clinical trials, which may be essential as we do not currently know if drugs that are effective at inhibiting white matter lesion formation also prevent subpial cortical lesion formation. In addition, cortical demyelination has been studied mainly in the context of MS and there is some evidence that it may be specific to MS (46), but IR-SWIET could be used to study larger cohorts with other inflammatory and non-inflammatory brain diseases to determine how specific subpial demyelination is to MS. Ultimately, IR-SWIET could be incorporated into clinical scans to improve accuracy of MS diagnosis and prognosis, and help to measure response to treatment.

Supplementary Material

Refer to Web version on PubMed Central for supplementary material.

Acknowledgments

Sources of support:

This research was supported by the Intramural Research Program of the National Institute of Neurological Disorders and Stroke, NIH. Erin Beck was supported by a Clinician Scientist Development Award and a Career Transition Fellowship Award from the National Multiple Sclerosis Society.

References

1. Brownell B, Hughes JT. The distribution of plaques in the cerebrum in multiple sclerosis. J Neurol Neurosurg Psychiatry. 1962;25:315–20. [PubMed: 14016083]
2. Bo L, Vedeler CA, Nyland HI, et al. Subpial demyelination in the cerebral cortex of multiple sclerosis patients. J Neuropathol Exp Neurol. 2003;62(7):723–32. [PubMed: 12901699]
3. Lucchinetti CF, Popescu BF, Bunyan RF, et al. Inflammatory cortical demyelination in early multiple sclerosis. N Engl J Med. 2011;365(23):2188–97. [PubMed: 22150037]
4. Calabrese M, Agosta F, Rinaldi F, et al. Cortical lesions and atrophy associated with cognitive impairment in relapsing-remitting multiple sclerosis. Arch Neurol. 2009;66(9):1144–50. [PubMed: 19752305]
5. Calabrese M, Poretto V, Favaretto A, et al. Cortical lesion load associates with progression of disability in multiple sclerosis. Brain. 2012;135(Pt 10):2952–61. [PubMed: 23065788]
6. Harrison DM, Roy S, Oh J, et al. Association of Cortical Lesion Burden on 7-T Magnetic Resonance Imaging With Cognition and Disability in Multiple Sclerosis. JAMA Neurol. 2015;72(9):1004–12. [PubMed: 26192316]
7. Calabrese M, Favaretto A, Poretto V, et al. Low degree of cortical pathology is associated with benign course of multiple sclerosis. Mult Scler. 2013;19(7):904–11. [PubMed: 23069877]
8. Treaba CA, Granberg TE, Sormani MP, et al. Longitudinal Characterization of Cortical Lesion Development and Evolution in Multiple Sclerosis with 7.0-T MRI. Radiology. 2019;291(3):740–9. [PubMed: 30964421]
9. Magliozzi R, Howell O, Vora A, et al. Meningeal B-cell follicles in secondary progressive multiple sclerosis associate with early onset of disease and severe cortical pathology. Brain. 2007;130(Pt 4):1089–104. [PubMed: 17438020]
10. Magliozzi R, Howell OW, Reeves C, et al. A Gradient of neuronal loss and meningeal inflammation in multiple sclerosis. Ann Neurol. 2010;68(4):477–93. [PubMed: 20976767]
11. Howell OW, Reeves CA, Nicholas R, et al. Meningeal inflammation is widespread and linked to cortical pathology in multiple sclerosis. Brain. 2011;134(Pt 9):2755–71. [PubMed: 21840891]
12. Choi SR, Howell OW, Carassiti D, et al. Meningeal inflammation plays a role in the pathology of primary progressive multiple sclerosis. Brain. 2012;135(Pt 10):2925–37. [PubMed: 22907116]
13. Geurts JJ, Pouwels PJ, Uitdehaag BM, et al. Intracortical lesions in multiple sclerosis: improved detection with 3D double inversion-recovery MR imaging. Radiology. 2005;236(1):254–60. [PubMed: 15987979]
14. Calabrese M, Filippi M, Rovaris M, et al. Morphology and evolution of cortical lesions in multiple sclerosis. A longitudinal MRI study. Neuroimage. 2008;42(4):1324–8. [PubMed: 18652903]
15. Absinta M, Rocca MA, Moiola L, et al. Cortical lesions in children with multiple sclerosis. Neurology. 2011;76(10):910–3. [PubMed: 21383327]
16. Seewann A, Kooi EJ, Roosendaal SD, et al. Postmortem verification of MS cortical lesion detection with 3D DIR. Neurology. 2012;78(5):302–8. [PubMed: 22218278]
17. Kilsdonk ID, Jonkman LE, Klaver R, et al. Increased cortical grey matter lesion detection in multiple sclerosis with 7 T MRI: a post-mortem verification study. Brain. 2016;139(Pt 5):1472–81. [PubMed: 26956422]
18. Nelson F, Poonawalla AH, Hou P, et al. Improved identification of intracortical lesions in multiple sclerosis with phase-sensitive inversion recovery in combination with fast double inversion recovery MR imaging. AJNR Am J Neuroradiol. 2007;28(9):1645–9. [PubMed: 17885241]
19. Sethi V, Yousry TA, Muhlert N, et al. Improved detection of cortical MS lesions with phase-sensitive inversion recovery MRI. J Neurol Neurosurg Psychiatry. 2012;83(9):877–82. [PubMed: 22807559]

20. Sethi V, Yousry T, Muhlert N, et al. A longitudinal study of cortical grey matter lesion subtypes in relapse-onset multiple sclerosis. J Neurol Neurosurg Psychiatry. 2016;87(7):750–3. [PubMed: 26272028]
21. Harel A, Ceccarelli A, Farrell C, et al. Phase-Sensitive Inversion-Recovery MRI Improves Longitudinal Cortical Lesion Detection in Progressive MS. PLoS One. 2016;11(3):e0152180. [PubMed: 27002529]
22. Marques JP, Kober T, Krueger G, et al. MP2RAGE, a self bias-field corrected sequence for improved segmentation and T1-mapping at high field. Neuroimage. 2010;49(2):1271–81. [PubMed: 19819338]
23. Kober T, Granziera C, Ribes D, et al. MP2RAGE multiple sclerosis magnetic resonance imaging at 3 T. Invest Radiol. 2012;47(6):346–52. [PubMed: 22543966]
24. Beck ES, Sati P, Sethi V, et al. Improved Visualization of Cortical Lesions in Multiple Sclerosis Using 7T MP2RAGE. AJNR Am J Neuroradiol. 2018.
25. Mainero C, Benner T, Radding A, et al. In vivo imaging of cortical pathology in multiple sclerosis using ultra-high field MRI. Neurology. 2009;73(12):941–8. [PubMed: 19641168]
26. Mainero C, Louapre C, Govindarajan ST, et al. A gradient in cortical pathology in multiple sclerosis by in vivo quantitative 7 T imaging. Brain. 2015;138(Pt 4):932–45. [PubMed: 25681411]
27. Nielsen AS, Kinkel RP, Madigan N, et al. Contribution of cortical lesion subtypes at 7T MRI to physical and cognitive performance in MS. Neurology. 2013;81(7):641–9. [PubMed: 23864311]
28. Louapre C, Govindarajan ST, Giannì C, et al. The association between intra- and juxtacortical pathology and cognitive impairment in multiple sclerosis by quantitative T. Neuroimage Clin. 2016;12:879–86. [PubMed: 27872810]
29. Nielsen AS, Kinkel RP, Tinelli E, et al. Focal cortical lesion detection in multiple sclerosis: 3 Tesla DIR versus 7 Tesla FLASH-T2. J Magn Reson Imaging. 2012;35(3):537–42. [PubMed: 22045554]
30. Pitt D, Boster A, Pei W, et al. Imaging cortical lesions in multiple sclerosis with ultra-high-field magnetic resonance imaging. Arch Neurol. 2010;67(7):812–8. [PubMed: 20625086]
31. Haacke EM, Cheng NY, House MJ, et al. Imaging iron stores in the brain using magnetic resonance imaging. Magn Reson Imaging. 2005;23(1):1–25. [PubMed: 15733784]
32. Fukunaga M, Li TQ, van Gelderen P, et al. Layer-specific variation of iron content in cerebral cortex as a source of MRI contrast. Proc Natl Acad Sci U S A. 2010;107(8):3834–9. [PubMed: 20133720]
33. Yao B, Bagnato F, Matsuura E, et al. Chronic multiple sclerosis lesions: characterization with high-field-strength MR imaging. Radiology. 2012;262(1):206–15. [PubMed: 22084205]
34. Duyn JH. The future of ultra-high field MRI and fMRI for study of the human brain. Neuroimage. 2012;62(2):1241–8. [PubMed: 22063093]
35. Stanisz GJ, Odrobina EE, Pun J, et al. T1, T2 relaxation and magnetization transfer in tissue at 3T. Magn Reson Med. 2005;54(3):507–12. [PubMed: 16086319]
36. Shin W, Gu H, Yang Y. Fast high-resolution T1 mapping using inversion-recovery Look-Locker echo-planar imaging at steady state: optimization for accuracy and reliability. Magn Reson Med. 2009;61(4):899–906. [PubMed: 19195021]
37. Gai ND, Butman JA. Modulated repetition time look-locker (MORTLL): a method for rapid high resolution three-dimensional T1 mapping. J Magn Reson Imaging. 2009;30(3):640–8. [PubMed: 19630081]
38. Gutteridge S, Ramanathan C, Bowtell R. Mapping the absolute value of M0 using dipolar field effects. Magn Reson Med. 2002;47(5):871–9. [PubMed: 11979565]
39. Rydberg JN, Riederer SJ, Rydberg CH, Jack CR. Contrast optimization of fluid-attenuated inversion recovery (FLAIR) imaging. Magn Reson Med. 1995;34(6):868–77. [PubMed: 8598814]
40. Gai ND, Nair G, Beck ES, Reich DS. Inversion recovery susceptiubility weighted imaging with enhanced T2 weighting (IR-SWIET): Application to multiple sclerosis lesions. Proc ISMRM. 2019.
41. Avants BB, Tustison NJ, Song G, et al. A reproducible evaluation of ANTs similarity metric performance in brain image registration. Neuroimage. 2011;54(3):2033–44. [PubMed: 20851191]

42. Cox RW. AFNI: software for analysis and visualization of functional magnetic resonance neuroimages. Comput Biomed Res. 1996;29(3):162–73. [PubMed: 8812068]

43. Beck ES, Maranzano J, Sati P, et al. Detection of cortical demyelination using multimodal high-resolution MRI and its correlation with clinical and MRI measures of disease. ACTRIMS 2019. 2019.

44. Sati P, Oh J, Constable RT, et al. The central vein sign and its clinical evaluation for the diagnosis of multiple sclerosis: a consensus statement from the North American Imaging in Multiple Sclerosis Cooperative. Nat Rev Neurol. 2016;12(12):714–22. [PubMed: 27834394]

45. Absinta M, Vuolo L, Rao A, et al. Gadolinium-based MRI characterization of leptomeningeal inflammation in multiple sclerosis. Neurology. 2015;85(1):18–28. [PubMed: 25888557]

46. Junker A, Wozniak J, Voigt D, et al. Extensive subpial cortical demyelination is specific to multiple sclerosis. Brain Pathol. 2020.

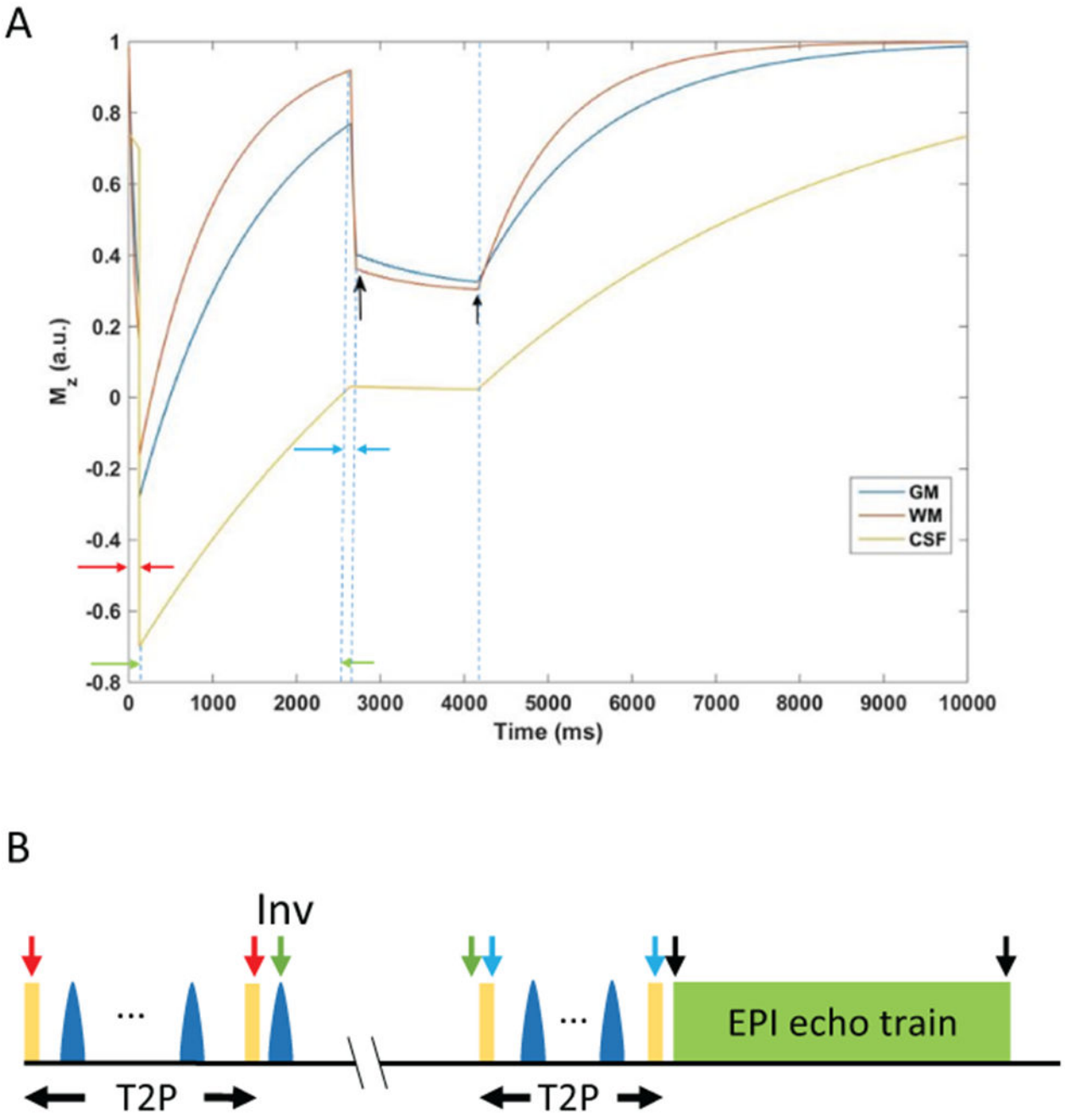

Figure 1.

Development of the inversion recovery susceptibility weighted imaging with enhanced T2 weighting (IR-SWIET) sequence. A) Mz evolution for IR-SWIET at steady-state. Arrows indicate beginning and end of each epoch. Black arrows indicate beginning and end of data acquisition. GM = gray matter, WM = white matter, CSF = cerebrospinal fluid. B) Schematic diagram for the IR-SWIET sequence. Arrows shown correspond to the magnetization epoch portrayed in (A).

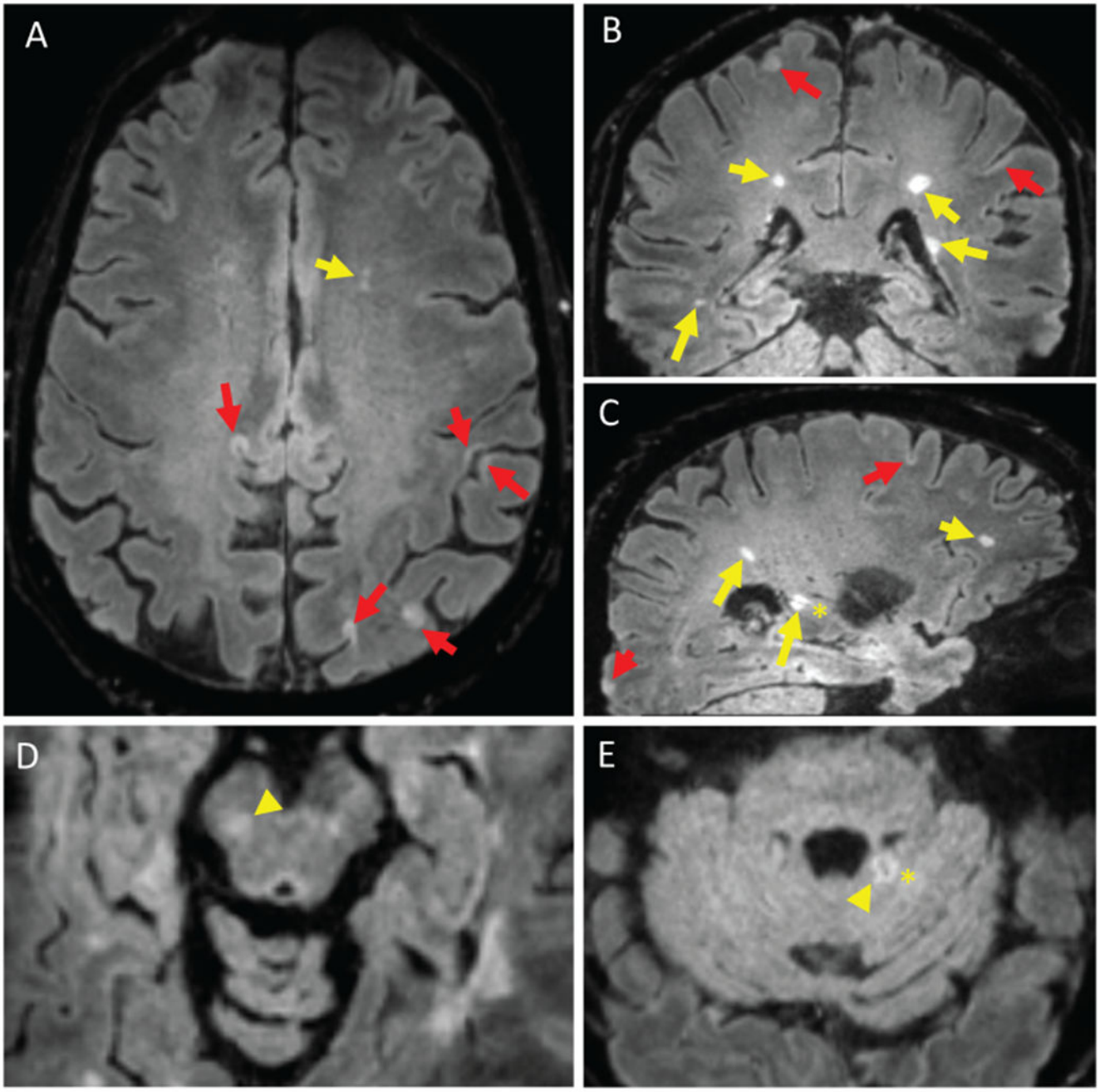

Figure 2.

Inversion recovery susceptibility weighted imaging with enhanced T_2 weighting (IR-SWIET) images. IR-SWIET is a 3D sequence reconstructed with isotropic voxels, allowing for reconstruction in axial (A), coronal (B), and sagittal (C) planes. IR-SWIET images have suppressed CSF signal, making cortical lesions easier to see. (A-C) White matter lesions (yellow arrows) and cortical lesions (red arrows) are conspicuous and central veins (asterisk) can be seen in some lesions. Lesions in the brainstem (D, yellow arrowhead) and cerebellum

(E, yellow arrowhead) are also observed. All images are medians of four IR-SWIET acquisitions.

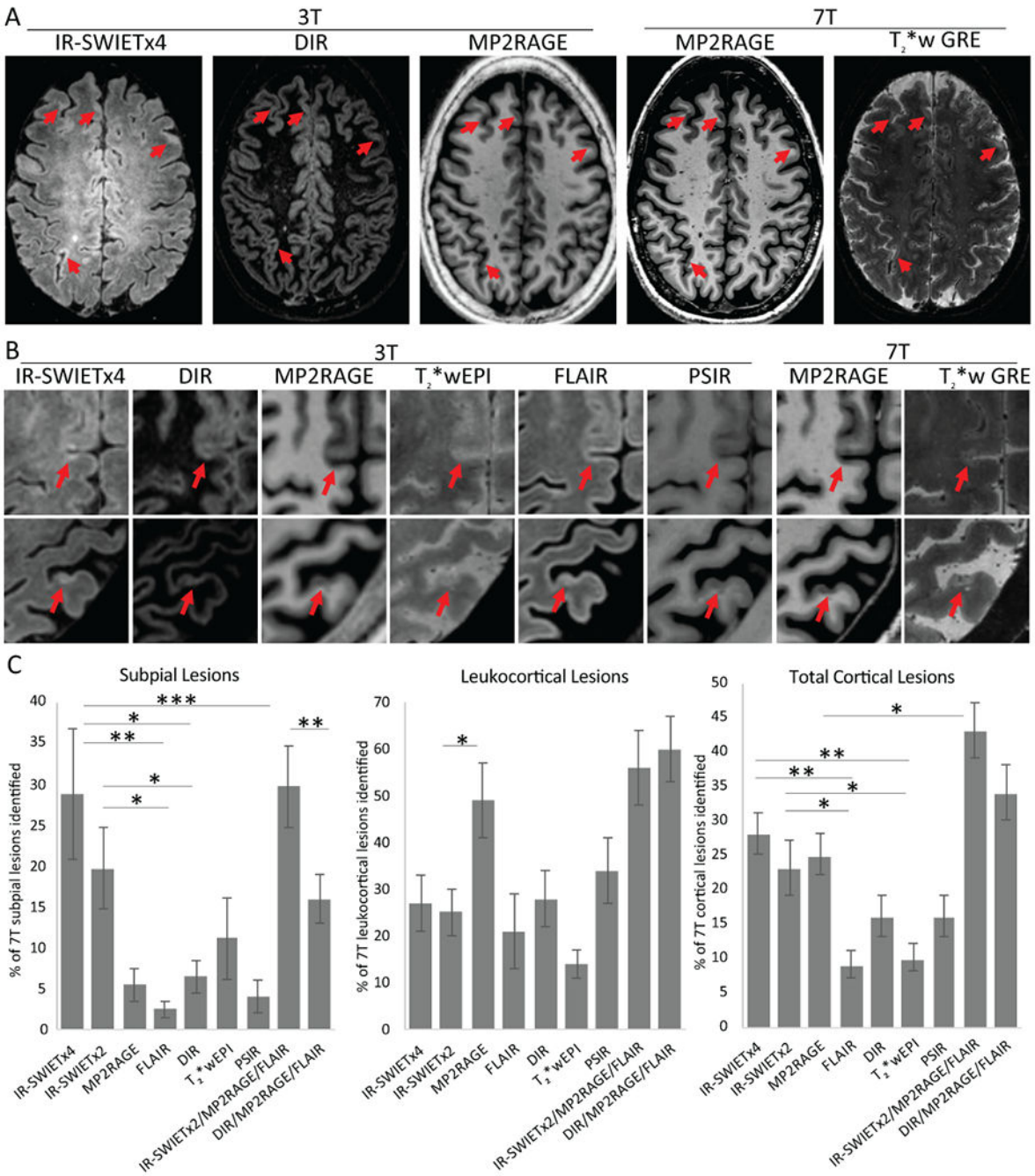

Figure 3.

IR-SWIET improves subpial lesion detection. A) Subpial lesions (red arrow) are well seen on IR-SWIET images compared to other 3T images and are confirmed as lesions on 7T images. B) High magnification view of two subpial lesions identified on IR-SWIET but which are more subtle on other 3T images and are confirmed on 7T images. C) Quantification of sensitivity of individual 3T sequences and 3T multicontrast reads compared to lesions identified on 7T images. *=p<0.05, **=p<0.01, ***=p<0.001, IR-SWIET – inversion recovery susceptibility weighted imaging with enhanced T_2 weighting

(x2 - median of two acquisitions, x4 – median of four acquisitions), DIR – double inversion recovery, MP2RAGE – magnetization-prepared 2 rapid gradient echo, T_2*wEPI – T_2* weighted segmented echo-planar imaging, FLAIR – fluid-attenuated inversion recovery, PSIR – phase-sensitive inversion recovery, GRE – gradient recalled echo.

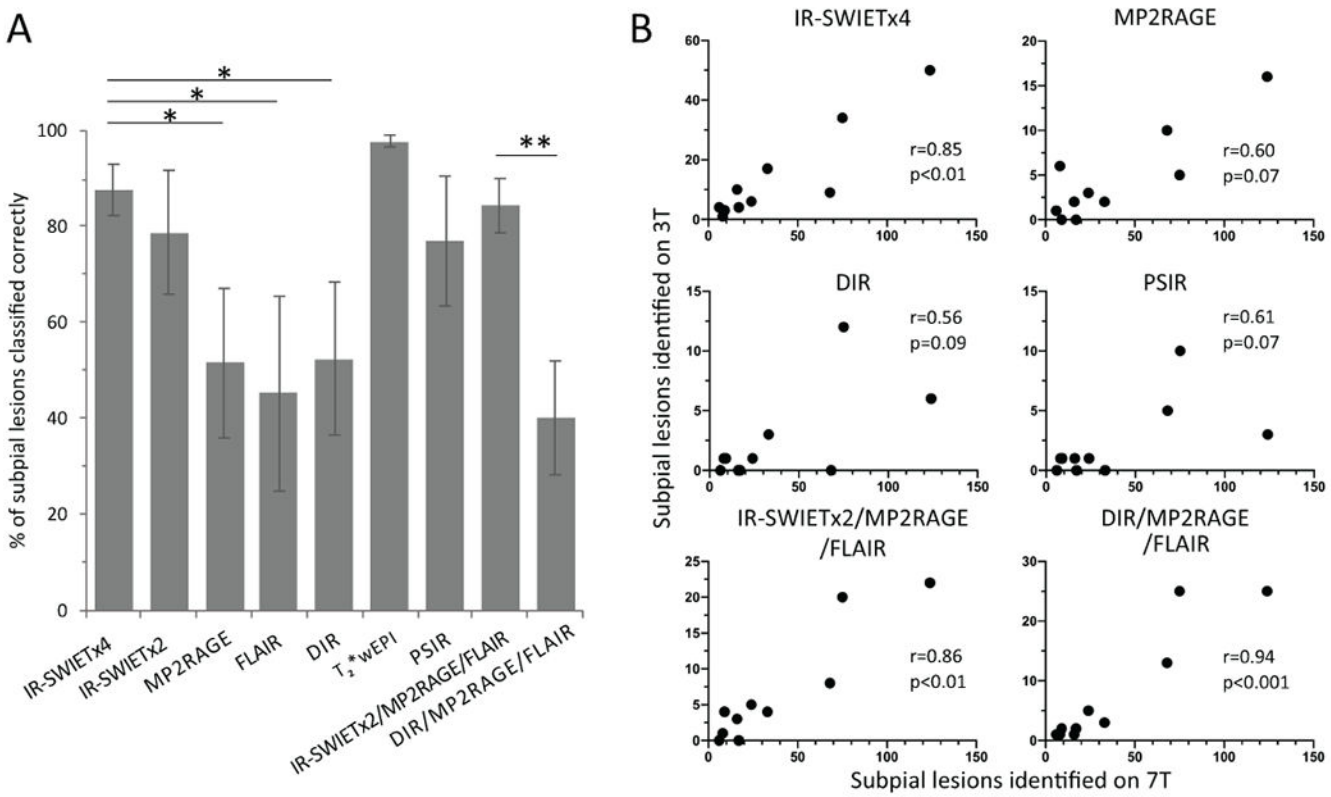

Figure 4.

IR-SWIET improves subpial classification and 3T-7T subpial correlation. A) Subpial lesion classification is more accurate on IR-SWIET than on MP2RAGE, FLAIR, and DIR, and IR-SWIETx2/MP2RAGE/FLAIR is more accurate than DIR/M2RAGE/FLAIR. *=p<0.05, **=p<0.01 B) Correlation between subpial lesions identified on 3T vs 7T is higher for IR-SWIETx4, IR-SWIETx2/MP2RAGE/FLAIR, and DIR/MP2RAGE/FLAIR than for MP2RAGE, DIR, or PSIR. IR-SWIET – inversion recovery susceptibility weighted imaging with enhanced T_2 weighting (x2 - median of two acquisitions, x4 – median of four acquisitions), DIR – double inversion recovery, MP2RAGE – magnetization-prepared 2 rapid gradient echo, T_2*wEPI – T_2* weighted segmented echo-planar imaging, FLAIR – fluid-attenuated inversion recovery, PSIR – phase-sensitive inversion recovery.

Table 1.

Sequence Parameters.

	3T						7T	
	IR-SWIET[1]	**DIR**[2]	**MP2RAGE**[3]	**T_2*wEPI**[4]	**FLAIR**[5]	**PSIR**[6]	**MP2RAGE**	**T_2*w GRE**[7]
Orientation	Sagittal	Sagittal	Sagittal	Sagittal	Sagittal	Axial	Axial	Axial
2D vs 3D	3D	3D	3D	3D	3D	2D	3D	2D
Voxel dimensions (mm)	0.8x0.8 (reconstructed at 0.64x0.64)	1.2x1.2	1x1	0.54x0.57	1x1	0.5x.0.53	0.5x0.5	0.5x0.5
Slice thickness (mm)	0.64	0.65	1	0.55	0.76	2	0.50	0.50
FOV	245 (SI) x229 (AP) x 160 (RL)	250 (SI) x 250 (AP) x 167 (RL)	256 (SI) x240 (AP) x176 (RL)	240 (SI) x 240 (AP) x 168 (RL)	224 (SI) x 224 (AP) x 237 (RL)	240 (AP) x 239 (RL) x 110 (SI)	224 (AP) x 168 (RL) x112 (SI)	240 (AP) x 168 (RL) x30 (SI)
TI (ms)	2650	2550/450	700/2500	NA	1650	400	800/2700	NA
TR/TE (ms)	58/32	5500/203	5000/2.9	54/29	4800/321	10010/17	6000/5	4095/11.4, 22.5, 33.6, 44.7, 55.8
Flip angle (°)	12	90	4/5	10	90	90	4/5	70
Scan time (min:sec)	5:08	10:44	8:16	4:15	4:55	8:30	10:32 (median of 4 acquisitions analyzed)	11:26 per volume x3 for full supratentorial coverage

[1] Inversion recovery susceptibility weighted imaging with enhanced T_2 weighting,

[2] Double inversion recovery,

[3] Magnetization-prepared 2 rapid gradient echo,

[4] T_2* weighted segmented echo-planar imaging,

[5] Fluid-attenuated inversion recovery,

[6] Phase-sensitive inversion recovery.

FOV – field of view, TI – inversion time, TR – repetition time, TE – echo time.

Table 2.

Cortical lesion identification.

	Subpial lesions			Leukocortical lesions			Total cortical lesions		
	Total	**Median (range)**	**Sensitivity (mean ± SEM)**	**Total**	**Median (range)**	**Sensitivity (mean ± SEM)**	**Total**	**Median (range)**	**Sensitivity (mean ± SEM)**
IR-SWIETx4	101	5 (0-38)	29 ± 8%	110	10 (0-35)	27 ± 6%	217	15 (5-56)	28 ± 3%
IR-SWIETx2	85	2 (0-41)	20 ± 5%	98	10 (0-31)	25 ± 5%	189	14 (2-49)	23 ± 4%
IR-SWIET	62	3 (0-26)	18 ± 5%	76	6 (0-22)	21 ± 7%	147	14 (1-33)	20 ± 4%
MP2RAGE	36	1 (0-13)	5 ± 2%	172	14 (0-44) †	49 ± 8% †	216	17 (1-54)	25 ± 3%
FLAIR	17	0 (0-7) **, †	2 ± 1% *,†	51	5 (0-11)	21 ± 8%	68	5 (0-17) **,†	9 ± 2% **,†
DIR	28	1 (0-15) *	6 ± 2% *, †	95	12 (0-20)	28 ± 6%	128	14 (0-28)	16 ± 3%
T_2*wEPI	42	2 (0-16)	11 ± 5% *	44	4 (0-10)	14 ± 3%	84	6 (0-25) **, †	10 ± 2% **, †
PSIR	13	1 (0-6) ***, †	4 ± 2% *	96	10 (0-17)	34 ± 7%	113	13 (0-21)	16 ± 3%
IR-SWIETx2/ MP2RAGE/ FLAIR	147	5 (0-63) ###	30 ± 5% ##,‡‡	225	17 (0-53)	56 ± 8%	380	24 (0-119) ###	43 ± 4% ##, ‡
DIR/ MP2RAGE/ FLAIR	83	3 (0-33)	16 ± 3% ##	231	18 (0-52) #	60 ± 7% #	300	24 (1-72)	34 ± 4% ##
7T	380	21 (6-124)		360	26 (1-84)		785	58 (17-201)	

* p<0.05 vs IR-SWIETx4,

** p<0.01 vs IR-SWIETx4,

*** p<0.001 vs IR-SWIETx4,

† p<0.05 vs IR-SWIETx2,

†† p<0.01 vs IR-SWIETx2,

‡ p<0.05 vs DIR/MP2RAGE/FLAIR,

‡‡ p<0.01 vs DIR/MP2RAGE/FLAIR,

# p<0.05 vs MP2RAGE,

p<0.01 vs MP2RAGE,

p<0.001 vs MP2RAGE.

IR-SWIET – inversion recovery susceptibility weighted imaging with enhanced T_2 weighting (x2 - median of two acquisitions, x4 – median of four acquisitions), DIR – double inversion recovery, MP2RAGE – magnetization-prepared 2 rapid gradient echo, T_2*wEPI – T_2* weighted segmented echo-planar imaging, FLAIR – fluid-attenuated inversion recovery, PSIR – phase-sensitive inversion recovery, GRE – gradient recalled echo.

Table 3.

Interrater reliability.

	% of lesions identified by both raters			Intraclass correlation coefficient		
	Subpial lesions	**Leukocortical lesions**	**Total cortical lesions**	**Subpial lesions**	**Leukocortical lesions**	**Total cortical lesions**
IR-SWIETx2	31	37	36	0.77	0.94	0.83
IR-SWIETx2/ MP2RAGE/ FLAIR	37	61	48	0.81	0.94	0.89
7T	40	52	45	0.95	0.93	0.91

IR-SWIETx2 – inversion recovery susceptibility weighted imaging with enhanced T_2 weighting, median of two acquisitions, MP2RAGE – magnetization-prepared 2 rapid gradient echo, FLAIR – fluid-attenuated inversion recovery.